Abstracts

Biomedical Laboratory Science

Comparative Effect of Amlodipine and Cilnidipine on Cardiac Remodeling and Diastolic Function in Dahl Salt-Sensitive Rats

Miwa Takatsu[1)], Takuya Hattori[1)], Tamayo Murase[1)], Masafumi Ohtake[1)], Miki Kato[2)], Keigo Nashima[2)], Chieko Nakashima[2)], Keiji Takahashi[1)], Kazumi Niinuma[3)], Shizuka Aritomi[3)], Toyoaki Murohara[4)], Kohzo Nagata[2)]

1) Department of Pathophysiological Laboratory Sciences, Nagoya University Graduate School of Medicine, Nagoya, Japan
2) Department of Medical Technology, Nagoya University School of Health Sciences, Nagoya, Japan
3) Research Center, Ajinomoto Pharmaceuticals Co. Ltd., Kawasaki, Japan
4) Department of Cardiology, Nagoya University Graduate School of Medicine, Nagoya, Japan

Introduction

The L/N-type calcium channel blocker (CCB) cilnidipine suppresses sympathetic nerve activity and has a superior renoprotective effect compared with L-type CCBs such as amlodipine. The cardioprotective action of cilnidipine has remained largely uncharacterized, however. We have now investigated the effects of cilnidipine, in comparison with amlodipine, on cardiac pathophysiology in rats with salt-sensitive hypertension.

Materials and Methods

Animals and experimental protocols: Dahl salt-sensitive (DS) rats fed a high-salt diet (8% NaCl) from 6 weeks of age were treated with vehicle (LVH group), amlodipine (3 mg/kg per day), or cilnidipine (3 mg/kg per day) from 7 to 11 weeks (n = 6, 10, and 10, respectively). DS rats maintained on a 0.36% NaCl diet after 6 weeks of age served as age-matched controls (CONT group, n = 6). At 11 weeks of age, all rats were anesthetized and were subjected to echocardiographic and hemodynamic analyses.

Blood pressure measurement and echocardiography: Systolic blood pressure (SBP) was measured weekly in conscious animals by tail-cuff plethysmography (BP-98A; Softron, Tokyo, Japan). At 11 weeks, rats were subjected to transthoracic echocardiography as previously described [1]. After echocardiography, cardiac catheterization was performed as described previously [2]. Left ventricular (LV) end-diastolic pressure (LVEDP) was determined and the time constant of isovolumic relaxation (tau) was calculated by the derivative method of Raff and Glantz, as described previously [3].

Histology and immunohistochemistry: LV tissue was fixed with ice-cold 4% paraformaldehyde for 48 to 72 h, embedded in paraffin wax, and processed for histology as described [4].To evaluate macrophage infiltration into the myocardium, we performed immunostaining for the monocyte-macrophage marker CD68 with frozen sections (thickness, 5 μm) that had been fixed with acetone.

Measurement of biochemical parameters: Plasma renin activity, plasma angiotensin II concentration, and serum aldosterone concentration were determined by radioimmunoassay as described previously [5].Urinary norepinephrine concentration was measured by high-performance liquid chromatography, and urinary norepinephrine excretion over 24 h was calculated as described previously [6].

Assay of superoxide production: NADPH-dependent superoxide production by homogenates of freshly frozen LV tissue was measured with an assay based on lucigenin-enhanced chemiluminescence as described previously [7]. Superoxide production in tissue sections was examined by staining with dihydroethidium (Sigma, St. Louis, MO, USA) as described [8].

*Assay of myocardial norepinephrine level*s: Norepinephrine levels in heart tissue were measured by high-performance liquid chromatography with electrochemical detection, as described previously [9].

Quantitative RT-PCR analysis: Total RNA was extracted from LV tissue and treated with DNase with the use of a spin-vacuum isolation kit (Promega, Madison, WI). Complementary DNA was synthesized from 2 μg of total RNA by reverse transcription (RT) with random primers (Invitrogen, Carlsbad, CA) and MuLV Reverse Transcriptase (Applied Biosystems, Foster City, CA). Real-time polymerase chain reaction (PCR) analysis was performed as previously described [10].

Western blot analysis: Protein levels in LV tissue were analyzed by Western blotting using specific antibodies as previously described [11].

Statistical analysis: Data are presented as means ± SEM. Differences among groups of rats at 11 weeks were assessed by one-way factorial analysis of variance (ANOVA); if a significant difference was detected, intergroup comparisons were performed with Fisher's multiple-comparison test. The time course of SBP was compared among groups by two-way repeated-measures ANOVA. A P value of < 0.05 was considered statistically significant.

Results

SBP was similar in all groups of rats at 6 weeks, but it was significantly higher in the vehicle-treated (LVH) group than in the CONT group at 7 weeks and thereafter. SBP was significantly reduced in the amlodipine (Aml)– and cilnidipine (Cil)–treated groups at 8 weeks and thereafter compared with that in the LVH group, but it did not differ between the Aml and Cil groups at any age. The ratios of heart or LV weight to tibial length, indices of cardiac and LV hypertrophy, respectively, were significantly increased in the LVH group compared with the CONT group at 11 weeks, and these effects were similarly attenuated in the Aml and Cil groups. Salt loading reduced plasma renin activity as well as the plasma angiotensin II and serum aldosterone concentrations in the LVH group, and these changes were not affected by treatment with either drug. Urinary norepinephrine excretion was markedly increased in the LVH group compared with the CONT group at 11 weeks, and this effect again was not influenced by drug treatment. Myocardial norepinephrine content was significantly decreased in the LVH group compared with the CONT group, but this change was reversed by both drugs. None of these measured parameters differed significantly between the Aml and Cil groups.

Echocardiography revealed that both LVDd and LVDs were decreased, and that IVST, LVPWT, LVFS, LV mass, and

relative wall thickness (RWT) were increased, in the LVH group compared with the CONT group. The increase in LV mass in the LVH group was similarly attenuated by both drug treatments, whereas that in RWT was inhibited to a greater extent in the Cil group than in the Aml group. The IRT, DcT, and tau, all of which are indices of LV relaxation, as well as the ratio of LVEDP to LVDd, an index of diastolic stiffness, were all increased in the LVH group compared with the CONT group. All of these changes were attenuated to a greater extent in the Cil group than in the Aml group.

Azan-Mallory staining revealed that fibrosis in perivascular and interstitial regions of the LV myocardium was increased in the LVH group compared with that in the CONT group. These increases in the extent of LV fibrosis were partially attenuated by treatment with amlodipine and were completely inhibited by treatment with cilnidipine. The abundance of collagen type I mRNA and the ratio of collagen type I to type III mRNA abundance, which correlates with myocardial diastolic stiffness, were increased in the left ventricle of rats in the LVH group, and this effect was attenuated to a greater extent in the Cil group than in the Aml group.

The amounts of TGF-β1 and CTGF mRNAs in the LV were significantly increased in the LVH group compared with the CONT group, and these effects were attenuated by amlodipine and to a greater extent by cilnidipine. Expression of the ACE gene was also significantly up-regulated in the LVH group compared with the CONT group, whereas that of the AT_{1A} receptor gene did not differ between these two groups. The overload-induced up-regulation of ACE gene expression was inhibited to a greater extent in the Cil group than in the Aml group, whereas expression of the AT_{1A} receptor gene was down-regulated in the Cil group but not in the Aml group. The abundance of the AT_1 receptor protein in the left ventricle showed a pattern similar to that of the AT_{1A} receptor mRNA in the four experimental groups.

Immunostaining for the monocyte-macrophage marker CD68 revealed that macrophage infiltration in the LV myocardium was increased in the LVH group compared with that in the CONT group and that this effect of salt loading was partially attenuated by treatment with amlodipine and was prevented by that with cilnidipine. The expression of inflammation-related genes in the left ventricle was also increased in the LVH group compared with the CONT group, and these effects were inhibited to a greater extent in the Cil group than in the Aml group.

Superoxide production in myocardial tissue sections revealed by staining with dihydroethidium as well as the activity of NADPH oxidase in LV homogenates were both markedly increased in the LVH group compared with the CONT group, and these effects were inhibited to a greater extent by cilnidipine than by amlodipine. The expression of genes for the components of NADPH oxidase was also up-regulated in the left ventricle of rats in the LVH group compared with the CONT group, and these effects were inhibited to a greater extent in the Cil group than in the Aml group.

Discussion

We have shown that both amlodipine and cilnidipine similarly attenuated hypertension and LV hypertrophy in DS rats, whereas cilnidipine ameliorated LV concentricity, fibrosis, and diastolic dysfunction to a greater extent than did amlodipine. The superior cardioprotective effects of cilnidipine were associated with more effective inhibition of cardiac oxidative stress and inflammation. In addition, whereas the suppression of the systemic renin-angiotensin system (RAS) by salt loading was not affected by cilnidipine or amlodipine, both the expression of ACE and AT_{1A} receptor mRNAs and that of AT_1 receptor protein in the heart of DS hypertensive rats were inhibited by cilnidipine but not by amlodipine, suggesting that the cardiac RAS was inhibited only by cilnidipine. However, the present study did not clarify whether the superior cardioprotective effects of cilnidipine are directly related to its N-type Ca^{2+} channel–blocking action in the heart. Further studies are required to determine the possible role of the N-type CCB activity, and thus of the sympatholytic effect, of cilnidipine in cardioprotection.

Conclusions

Cilnidipine attenuated LV fibrosis and diastolic dysfunction as well as LV concentricity to a greater extent than did amlodipine in DS rats. The superior cardioprotective action of cilnidipine is likely attributable, at least in part, to the greater antioxidant and anti-inflammatory effects associated with inhibition of cardiac RAS gene expression observed with this drug.

References

[1]Hayashi K, Kimata H, Obata K*, et al.* Xanthine oxidase inhibition improves left ventricular dysfunction in dilated cardiomyopathic hamsters. *J Card Fail*. 2008;14:238-244.

[2]Kato MF, Shibata R, Obata K*, et al.* Pioglitazone attenuates cardiac hypertrophy in rats with salt-sensitive hypertension: role of activation of AMP-activated protein kinase and inhibition of Akt. *J Hypertens*. 2008;26:1669-1676.

[3]Nagata K, Iwase M, Sobue T*, et al.* Differential effects of dobutamine and a phosphodiesterase inhibitor on early diastolic filling in patients with congestive heart failure. *J Am Coll Cardiol*. 1995;25:295-304.

[4]Nagata K, Somura F, Obata K*, et al.* AT1 receptor blockade reduces cardiac calcineurin activity in hypertensive rats. *Hypertension*. 2002;40:168-174.

[5]Yamada Y, Tsuboi K, Hattori T*, et al.* Mechanism underlying the efficacy of combination therapy with losartan and hydrochlorothiazide in rats with salt-sensitive hypertension. *Hypertens Res*. 2011;34:809-816.

[6]Ito K, Hirooka Y, Sunagawa K. Acquisition of brain Na sensitivity contributes to salt-induced sympathoexcitation and cardiac dysfunction in mice with pressure overload. *Circ Res.* 2009;104:1004-1011.

[7]Nagata K, Obata K, Xu J*, et al.* Mineralocorticoid receptor antagonism attenuates cardiac hypertrophy and failure in low-aldosterone hypertensive rats. *Hypertension*. 2006;47:656-664.

[8]Elmarakby AA, Loomis ED, Pollock JS*, et al.* NADPH oxidase inhibition attenuates oxidative stress but not hypertension produced by chronic ET-1. *Hypertension.* 2005;45:283-287.

[9]Li W, Knowlton D, Van Winkle DM*, et al.* Infarction alters both the distribution and noradrenergic properties of cardiac sympathetic neurons. *Am J Physiol Heart Circ Physiol*. 2004;286:H2229-2236.

[10]Somura F, Izawa H, Iwase M*, et al.* Reduced myocardial sarcoplasmic reticulum Ca(2+)-ATPase mRNA expression and biphasic force-frequency relations in patients with hypertrophic cardiomyopathy. *Circulation*. 2001;104:658-663.

[11]Xu J, Nagata K, Obata K*, et al.* Nicorandil promotes myocardial capillary and arteriolar growth in the failing heart of Dahl salt-sensitive hypertensive rats. *Hypertension*. 2005;46:719-724.

Author address

E-Mail: takatsu.miwa@f.mbox.nagoya-u.ac.jp

HO-1-Independent Anti-Allergic Action of Chrysin

Ayaka Teranishi[1)], Miyoko Matsushima[1, 2)], Akemi Mori[1)], Haruka Nose[2)], Nanako Ogasawara[1)], Yukiko Yamamoto[1)], Takehiro Yamaguchi[2)], Tsutomu Kawabe [1, 2)]

1) Department of Pathophysiological Laboratory Sciences, Nagoya University Graduate School of Medicine, Nagoya, Japan
2) Department of Medical Technology, Nagoya University School of Health Sciences, Nagoya, Japan

Intoroduction

Flavonoids are a group of polyphenolic compounds that are found in many fruits, vegetables, and beverages, including wine and tea. Flavonoids possess anti-oxidant, anti-tumor, anti-angiogenic, anti-inflammatory, anti-allergic, and anti-viral activities, and more than 4,000 different flavonoids have been identified to date . Flavonoids consist of two aromatic rings (A and B rings) that are joined by three carbons (C ring) [1].

We previously demonstrated that one of the flavonoids, quercetin exerted anti-allergic activity via heme oxygenase (HO)-1 activity in mast cells [2]. HO is the rate-limiting enzyme in the catabolism of heme. It breaks down the porphyrin ring to yield equimolar amounts of biliverdin, free iron (Fe^{2+}), and carbon monoxide (CO) [3]. In mammals, biliverdin is rapidly converted by biliverdin reductase into bilirubin. HO-1 is induced ubiquitously in response to oxidative stress and is involved in a multitude of signaling pathways [4].

Chrysin is a natural flavonoid contained in fruits and honey and exerts anti-allergic [5] and anti-tumor [6] activities although their precise mechanisms of action are unclear. Several studies have been reported that chrysin was not involved in the modification of mitogen-activated protein kinases (MAPKs) signaling pathway in IgE-stimulated mast cells whereas quercetin inhibited phosphorylation of MAPKs [7, 8]. These observations suggested that chrysin and quercetin might exert inhibitory effects through a different mechanism on signal transduction pathways.

In this study, we investigated the mechanism by which chrysin could exhibit an anti-allergic activity in murine mast cells. We also investigated the involvement of HO-1 in the inhibitory effect of chrysin on mast cell activation in murine mast cells.

Materials and Methods

Animals: Balb/c mice were maintained in a temperature-(22-24°C), humidity-(55±5%) and light-(12 hour light-dark cycle; lights on at 7:00) regulated room with food and water *ad libitum*. All procedures were performed with the approval of the Animal Experimentation Committee, Graduate School of Medicine, Nagoya University in accordance with the Guidelines for Animal Experimentation of Nagoya University.

***Cell Culture*:** RBL-2H3 cells were maintained in MEM supplemented with 10% fetal calf serum, 100 U/ml penicillin, and 100 μg/ml streptomycin. For preparation of bone marrow-derived mast cells (BMMC), bone marrow cells were obtained from the female of 7-week-old Balb/c mice, and cultured for 6 weeks in RPMI 1640 supplemented with 10% FCS, 20 ng/ml mouse IL-3, 100 U/ml penicillin, and 100 μg/ml streptomycin.

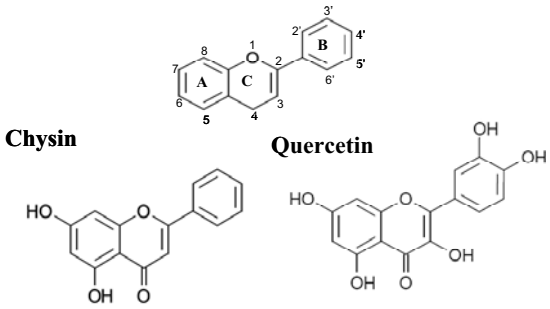

Fig. 1. Basic structure of flavonoids and the structure of chrysin and quercetin.

***Cell Activation*:** Cells (2×10^5 cells/ml) were plated and treated with chrysin for the indicated times and then stimulated with thapsigargin (10 μM) or A23187 (5×10^{-7} M) for 15 min. For IgE-mediated stimulation, cells were incubated with 0.1 μg/ml of mouse anti-dinitrophenyl IgE (αDNP-IgE) for 2 h and then stimulated with 0.1 μg/ml of DNP-bovine serum albumin (BSA) for 30 min.

***β-hexosaminidase Release Assay*:** The equal volume of supernatant and 1 mM p-nitrophenyl-N-acetyl-β-D-glucosaminide were added and incubated for 1 h at 37°C. After adding 0.1 M carbonate buffer, pH 10.5., the absorbance at 405 nm was measured. β-hexosaminidase release was expressed as a percentage of the total β-hexosaminidase activity, and the spontaneous release was subtracted from stimulated cell release.

***Western Blotting*:** 20 μg of protein was subjected to SDS-PAGE and transferred to polyvinylidene difluoride membranes. The membrane was incubated with 4% skim milk for 1 h at room temperature. The membrane was then incubated with primary antibodies overnight at 4°C. Subsequently, the membrane was incubated with either anti-rabbit IgG or anti-mouse IgG antibodies conjugated with horse radish peroxidase for 1 h at room temperature. The specific protein bands on the membrane were visualized using the Enhanced Chemiluminescence Kit (GE Healthcare Bioscience, Buckinghamshire, UK) according to the recommendations of the manufacturer.

RT-PCR, Quantitative real-time PCR: Total RNA was isolated using TRIZOL reagent and reverse-transcribed to cDNA using random hexamers and SuperScript II according to the manufact -ufacturer's instructions. cDNA was amplified with Taq polymerase using 28 cycles for b-actin, 30 cycles for HO-1, 35 cycle for TNF-a and IL-4 under the following conditions: denaturation at 94°C for 30 s, annealing at 55°C (β-actin) or 60°C (HO-1, IL-4) or 58°C (TNF-α) for 30 s, and extension at 72°C for 30 s.

Quantitative real-time PCR was performed on the ABI 7000 Sequence Detector (Applied Biosystems, FosterCity, CA,

USA). Primersand probes for HO-1, TNF-α and glyceraldehyde-3-phosphate dehydrogenase (GAPDH) were obtained from TaqManGene Expression Assays (Applied Biosystems, FosterCity, CA, USA).

Results

Chrysin inhibited degranulation in RBL-2H3 cells

Exposure of cells for 15 min to chrysin resulted in a concentration-dependent inhibition in degranulation from RBL-2H3 cells after stimulation with A23187, thapsigargin, or IgE. Chrysin strongly inhibited thapsigargin-induced degranulation whereas the extent of inhibition on A23187- or IgE-mediated degranulation by chrysin was much weaker. Quercetin, which is known to exhibit HO-1-dependent anti-allergic activity, also inhibited A23187-, thapsigargin-, or IgE-mediated degranulation. The extent of inhibition on A23187- or IgE-mediated degranulation by quercetin was more pronounced than chrysin. Chrysin and quercetin did not affect spontaneous degranulation and had no significant cytotoxicity in RBL-2H3 cells at the concentrations used.

Chrysin suppressed TNF-α and IL-4 mRNA expression in RBL-2H3 cells

We examined the effect of chrysin on tumor necrosis factor (TNF)-α and IL-4 mRNA expression stimulated with A23187 or IgE. The expression of TNF-α and IL-4 mRNA was increased in A23187- or IgE -stimulated RBL-2H3 cells, and robust inhibition was observed by chrysin treatment although chrysin showed weak inhibition of degranulation in A23187- or IgE-stimulated RBL-2H3 cells. These findings suggest that the inhibitory effect of chrysin could be superior to cytokine production rather than degranulation.

HO-1 expression induced by chrysin in RBL-2H3 cells

We previously demonstrated that quercetin exhibited anti-allergic action via induction of HO-1. We next examined expression levels of HO-1 mRNA and protein in RBL-2H3 cells cultured with chrysin by quantitative real-time PCR and western blot. Unexpectedly, the expression levels of HO-1 were not increased after exposure to chrysin. At the concentration of 50 μM of chrysin, significant decrease of HO-1 expression was observed, as compared with that of control.

Effect of HO-1 on degranulation in RBL-2H3 cells after exposure to chrysin

To investigate the involvement of HO-1 in the inhibitory activity of chrysin, we used tin protoporphyrin IX (SnPP), an HO-1 inhibitor. RBL-2H3 cells were exposed to SnPP for 1 h with a 15-min incubation of chrysin before stimulation. The inhibition of degranulation by chrysin was maintained despite the addition of SnPP, suggesting that the inhibition of degranulation by chrysin might be mediated via HO-1-independent pathway.

Effect of chrysin on HO-1 induction by hemin or quercetin in RBL-2H3 cells

Since we observed the reduction of HO-1 expression after exposure to chrysin at the concentration of 50 μM, we hypothesize that chrysin might transcriptionally regulate the expression of HO-1. We next investigated the effect of chrysin on HO-1 induction induced by quercetin or hemin, a HO-1 inducer, in RBL-2H3 cells. Chrysin decreased both quercetin- and hemin-induced HO-1 expression at the mRNA and protein levels.

Discussion

In this study, we demonstrated that the anti-allergic effect of chrysin was mediated via HO-1-independent pathway in murine mast cells. We also demonstrated that chrysin was able to decrease the expression of HO-1 induced by quercetin or hemin.

First, we investigated the inhibitory effect of chrysin on degranulation and the expression of TNF-α and IL-4 mRNA stimulated by A23187, thapsigargin, or IgE. Chrysin strongly inhibited thapsigargin-induced degranulation whereas the inhibition of A23187- or IgE-induced degranulation was weak. Since thapsigargin, an endoplasmic reticular Ca^{2+}-ATPase inhibitor, activates mast cells due to the elevation of cytosolic calcium levels, suggesting that chrysin might affect the calcium mobilization in mast cells.

Nuclear factor erythroid 2-related factor 2 (Nrf2) is involved in cellular protection against oxidative stress through antioxidant response element (ARE) -directed induction of several phase 2 detoxifying and antioxidant enzymes, including HO-1. HO-1 is also under the control of the transcription factor, broad complex-tramtrack-bric-a-brac (BTB) and Cap'n'collar (CNC) homology (Bach) 1, which repress the transcription HO-1 [9]. We have previously reported that quercetin upregulated HO-1 expression with the translocation of Nrf2, leading to anti-allergic effect in rodent mast cells [2]. We observed the reduction of quercetin- or hemin-induced HO-1 expression by chrysin, suggesting that chrysin might regulate the activation of Bach1 or Nrf2. It has been reported that genistein, also one of the flavonoids, blocked nuclear export of Bach1, thus allowing Nrf2 stays in cytoplasm [10]. This finding leads us to consider the possibility that chrysin might regulate Nrf2-Bach1 interaction. Further studies have to be elucidated how chrysin negatively regulates the expression of HO-1.

Conclusion

In the present study, our results demonstrated that chrysin mediated anti-inflammatory effects via HO-1-independent pathway in mast cells. To elucidate the molecular mechanism of anti-allergic effect by chrysin may well lead to promising new therapeutic strategies for promoting not only anti-allergic but also a wide range of anti-inflammatory therapy.

References

[1] Middleton, E. et al., (2000) *Pharmacol Rev* **52**, 673-751
[2] Matsushima, M. et al., (2009) *Inflamm Res* **58**, 705-715
[3] Gozzelino, R. et al., (2010) *Annu Rev Pharmacol Toxicol* **50**, 323-354
[4] Wagener, F. A. et al., (2003) *Pharmacol Rev* **55**, 551-571
[5] Bae, Y. et al., (2011) *Toxicol Appl Pharmacol* **254**, 56-64
[6] Samarghandian, S. et al., (2011) *Clinics* **66**, 1073-1079
[7] Itoh, T. et al., (2009) *Bioorg Med Chem* **17**, 5374-5379
[8] Min, Y. D. (2007) *Inflamm Res* **56**, 210-215
[9] Paine, A. et al., (2010) *Biochem Pharmacol* **80**, 1895-1903
[10] Kaspar, J. W. et al., (2010) *J Biol Chem* **285**, 153-162

Author address

E-Mail: teranishi.ayaka@a.mbox.nagoya-u.ac.jp

(-)-Epigallocatechin-3-gallate prevents doxorubicin-induced overexpression of P-glycoprotein through inhibition of MEK/ERK signaling pathway in HepG2 Cells

Hana Satonaka, Kumiki Ishida, Yuki Komori, Sakiko Arisawa, Jun Ueyama, Shinya Wakusawa

Department of Medical Technology, Nagoya University Graduate School of Health Sciences

Introduction

(-)-Epigallocatechin-3-gallate (EGCG) is the most abundant component of tea catechins, and it reportedly has various biological and pharmacological actions such as antioxidative and iron chelating activities. Additionally, EGCG has been suggested to inhibit the transport function of P-glycoprotein (P-gp) via direct action on it or antioxidative action [1,2]. P-gp is an efflux pump that extrudes chemotherapeutic agents out of the cells, decreasing their intracellular concentrations, and causing multidrug resistance (MDR) against anti-tumor chemotherapy. Therefore, modulations of the function and/or expression of P-gp are expected to improve the effect of anti-cancer chemotherapy.

In this study, we investigated whether EGCG acts as an inhibitor of the overexpression of P-gp in HepG2 cells. Further, to elucidate its mechanisms, we investigated the signal transduction system involved in the inhibitory action of EGCG on the up-regulation of P-gp induced by doxorubicin (DOX).

Materials and Methods

Cell culture. Human hepatoma HepG2 cells were cultured in Dulbecco's modified Eagle's medium (Sigma) supplemented with 5% (v/v) heat-inactivated fetal calf serum (BioWest) and 100 U/mL of penicillin, 100 μg/mL of streptomycin, and 0.25 μg/mL of amphotericin B (Invitrogen).

Rhodamin 123 (R123) uptake assay. After cells were incubated for 30 min with 3μM R123, intracellular R123 was extracted with ethanol and its fluorescence intensity was measured Ex; 480 nm, Em; 538 nm).

RT-PCR. After total RNA was isolated using TRIzol Reagent (Invitrogen), cDNA was prepared using RNA reverse transcriptase (ReverTra Ace, TOYOBO, Japan). Then, polymerase chain reaction (PCR) was carried out using specific PCR primers for MDR1 and GAPDH obtained from Hokkaido System Science (Sapporo, Japan).

Western blotting. P-gp was detected with the C219 anti-MDR1 P-gp mouse monoclonal antibody (Centocor). Total- and phosphorylated-proteins of ERK, p38 MAP kinase, and Akt were detected using respective specific antibodies obtained from Cell Signaling Technology.

Statistical analysis. Data are expressed as the mean ± S.D. Statistical analyses were performed using Student's t-test after a test for equality of variance. $P < 0.05$ was considered statistically significant

Results

Inhibition of DOX-induced MDR1 gene expression and P-gp expression by EGCG.

MDR1 gene expression was significantly induced by 24-hr treatment with DOX. While EGCG did not influence MDR1 gene expression by itself, it significantly suppressed the induction by DOX. The expression of P-gp was significantly increased by DOX, and the induction was markedly suppressed by EGCG (Figure 1).

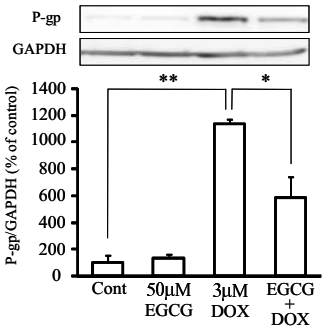

Figure 1. EGCG inhibits DOX-induced overexpression of P-gp in HepG2 cells.

HepG2 cells were exposed to 3 μM DOX in the presence or absence of 50 μM EGCG for 24 h. Then, whole cell lysates were used for Western blot analysis of P-gp. The photograph is typical of three independent experiments. Column graph data are expressed as the mean ± S.D. (n=3). *P<0.05, **P<0.01.

Reversal of R123 uptake in cells pretreated with EGCG and DOX.

To evaluate the effect on P-gp function in cells pretreated with DOX and EGCG, we examined the effect of combined pretreatment with EGCG and DOX on the uptake of R123. While the uptake of R123 was significantly decreased in DOX-pretreated cells, the uptake in the cells pretreated with EGCG combined with DOX was partially reversed.

Effects of inhibitors for MAP kinases and PI3K/Akt signaling on the DOX-induced MDR1 gene expression.

DOX-induced up-regulation of MDR1 mRNA was significantly suppressed by LY294002 (a PI3K inhibitor) and SB202190 (a p38 MAPK inhibitor), and slightly-suppressed by U0126 (a MEK1/2 inhibitor). SP600125 (a JNK inhibitor) barely influenced the levels in basal and stimulated conditions.

Effects of LY294002, SB202190, U0126 and SP600125 on P-gp level.

SB202190 and U0126 significantly decreased P-gp levels by combined treatment with DOX. On the other hand, LY294002 and SP600125 did not affect P-gp levels in combination with DOX (Figure 2).

Effects of EGCG on the phosphorylation of ERK, Akt, and p38 MAPK..

DOX significantly induced the phosphorylation of ERK, Akt, and p38 MAPK against the total level. EGCG inhibited DOX-induced phosphorylation of ERK and Akt, though it did not

affect the total level. On the other hand, EGCG did not affect DOX-induced phosphorylation of p38 MAPK (Figure 3).

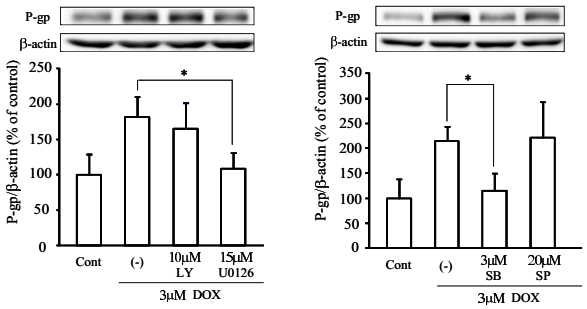

Figure 2. Effects of LY294002, U0126, SB202190, and SP600125 on DOX-induced overexpression of P-gp in HepG2 cells.

HepG2 cells were exposed to 3 μM DOX in the presence or absence of LY294002 (LY, 10 μM), U0126 (15 μM), SB202190 (SB, 3 μM), and SP600125 (SP, 20 μM) for 20-24 h. Then, whole cell lysates were used for Western blot analysis of P-gp. The photograph is typical of three independent experiments. Column graph data are expressed as the mean ± S.D. (n=3). *P<0.05.

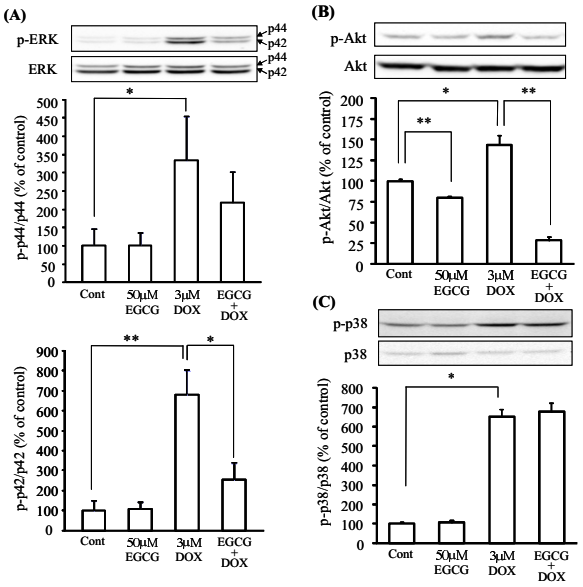

Figure 3. Effects of EGCG on the phosphorylation of ERK, Akt, and p38 MAPK in DOX-treated HepG2 cells.

HepG2 cells were exposed to 3 μM DOX in the presence or absence of 50 μM EGCG for 20-24 h. Then, whole cell lysates were used for Western blot analysis of phosphorylated ERK (p-ERK) (A), phosphorylated Akt (p-Akt) (B), and phosphorylated p38 MAPK (p-p38) (C). Total protein level was also detected with each specific antibody. The photograph is typical of three independent experiments. Column graph data are expressed as the mean ± S.D. (n=3). *P<0.05, **P<0.01.

Discussion

The results showed that EGCG inhibited P-gp overexpression in DOX-treated cells through inhibiting the induction of MDR1 gene expression. Our results also indicated that MDR1 gene overexpression by DOX depended on the activation of PI3K/Akt, MEK/ERK, and p38 MAPK signaling systems. However the P-gp expression was not affected by a PI3K/Akt inhibitor and therefore it was suggested that it is not directly dependent on the PI3K/Akt signaling system. Further, although EGCG inhibits both Akt phosphorylation and MDR1 gene overexpression, its inhibitory action on the PI3K/Akt pathway seemed to scarcely contribute to the suppression of P-gp overexpression. As for MEK/ERK signaling, EGCG partially inhibited DOX-induced activation of the MEK/ERK pathway along with decreasing the expression of MDR1 gene and P-gp. Then it was suggested that EGCG may prevent P-gp overexpression through the inhibitory action on MEK/ERK activation. As for p38 MAPK, several studies reported that EGCG inhibited its activity [3-5] and its negative effect has also been reported [6]. In the present study, as EGCG did not affect the activation of p38 MAPK by DOX in HepG2 cells, it clearly indicated that the effect of EGCG on P-gp overexpression is independent of the inhibitory action on p38 MAPK signaling pathway. Thus, it was suggested that EGCG partially inhibits the acquisition of P-gp-dependent multidrug resistance through the inhibition of MEK/ERK signaling pathway.

Conclusion

We showed that EGCG antagonized induction of P-gp in DOX-treated cells through inhibiting MDR1 gene overexpression. As the molecular bases of the phenomenon, we showed that EGCG inhibited DOX-induced activation of PI3K/Akt and MEK/ERK pathways and that P-gp induction by DOX was dependent on MEK/ERK and p38 MAPK. Therefore, it was suggested that EGCG suppressed DOX-induced P-gp overexpression partially through the inhibition of MEK/ERK signaling pathway.

References

[1] Mei Y, Wei D, Liu J. Reversal of multidrug resistance in kb cells with tea polyphenol antioxidant capacity. Cancer Biol Ther. 2005; 4: 468-473.

[2] Qian F, Wei D, Zhang Q, Yang S. Modulation of P-glycoprotein function and reversal of multidrug resistance by (-)-epigallocatechin gallate in human cancer cells. Biomed Pharmacother. 2005; 59: 64-69.

[3] Chen W, Dong Z, Valcic S, Timmermann BN, Bowden GT. Inhibition of ultraviolet B--induced c-fos gene expression and p38 mitogen-activated protein kinase activation by (-)-epigallocatechin gallate in a human keratinocyte cell line. Mol Carcinog. 1999; 24: 79-84.

[4] Li H-L, Huang Y, Zhang C-N, Liu G, Wei Y-S, Wang A-B, Liu Y-Q, Hui R-T, Wei C, Williams GM, Liu D-P, Liang CC. Epigallocathechin-3 gallate inhibits cardiac hypertrophy through blocking reactive oxidative species-dependent and -independent signal pathways. Free Radic Biol Med 2006; 40: 1756-1775.

[5] Hong MH, Kim MH, Chang HJ, Kim NH, Shin BA, Ahn BW, Jung YD. (-)-Epigallocatechin-3-gallate inhibits monocyte chemotactic protein-1 expression in endothelial cells via blocking NF-kappaB signaling. Life Sci. 2007; 80: 1957-1965.

[6] Yamauchi J, Takai S, Matsushima-Nishiwaki R, Hanai Y, Doi T, Kato H, Ogura S, Kato K, Tokuda H, Kozawa O. (-)-epigallocatechin gallate inhibits prostaglandin D2-stimulated HSP27 induction via suppression of the p44/p42 MAP kinase pathway in osteoblasts. Prostaglandins Leukot Essent Fatty Acids. 2007; 77: 173-179.

Author address

E-Mail: satonaka.hana@f.mbox.nagoya-u.ac.jp

THE POSITIVE ROLE OF C-MYB IN SPHK1 OVEREXPRESSION OF MOUSE ERYTHROLEUKEMIA CELLS

Misa Kobayashi[1)], Hiromi Ito[1)], Kazumi Hagiwara[1)], Asuka Hoshikawa[1)], Naoki Mizutani[1)], Keiko Tamiya-Koizumi[1)] Akira Takagi[1)], Tetsuhito Kojima[1)], Motoshi Suzuki[2)], Mitsuhiro Nakamura[3)], Yoshiko Banno[4)], and Takashi Murate[1)]

1) Department of Medical Technology, Nagoya University Graduate School of Health Sciences, Nagoya, Japan
2) Division of Molecular Carcinogenesis, Nagoya University Graduate School of Medicine, Nagoya, Japan
3) Department of Drug Information, Gifu Pharmaceutical University, Gifu, Japan
4) Department of Dermatology, Gifu Graduate School of Medicine, Gifu, Japan

Introduction

Sphingolipid (SPL) is a complex lipid containing an amide-linked fatty acid and sphingoid base. Recently, SPLs such as ceramide, sphingosine and sphingosine 1-phospahte (S1P), and ceramide 1-phosphate are considered as intracellular or intercellular signaling molecules in numerous biological processes (1). Sphingolipid rheostat model, where he balance between ceramide and S1P determines cell's fate has been proposed (2). Ceramide acts as a signaling molecule leading to apoptosis, growth arrest, cell differentiation and inflammation, whereas S1P mostly works as an inhibitor of apoptosis and stimulator of cell proliferation.

S1P is produced by sphingosine kinases 1 and 2. SPHK1 expression not only stimulates proliferation and protects from apoptosis, but also induces tumor formation in some cases. On the contrary, overexpression of SPHK2 suppresses cell growth and induces apoptosis. Thus, SPHKs play an important role in cancer growth and survival. Previous reports including ours have shown increased SPHK1 expression of various cancer and leukemia cells. Considering the role of sphingolipid metabolic enzymes as the chemotherapy sensor, the elucidation of SPHK1 expression mechanism is clinically important.

The mouse erythroleukemia cell line caused by the Friend virus (Friend cells) has been extensively studied, because of the suitable model of virus oncogenesis (3) and also because of high inducibility toward erythroid lineage by chemical inducers. The sequential changes of protooncogenes (*c-Myb, Fli-1 and Pu.1*) and cell cycle regulators (CDK2,4 and 6) have been reported.

Recently, le Scolan *et al.* reported that overexpression of SPHK1 is an oncogenic event in Friend cell lines (4). However, it remains to be determined how this overexpression is induced and whether HMBA-induced differentiation affects this overexpression. We approached these issues by establishng wild-type (WT) and dominant negative (DN) SPHK1- and SPHK2-transfected Friend cells and HMBA-resistant Friend cells (R cells). We further analyzed mouse *Sphk1* transcription mechanism in Friend cells. Our analysis revealed that the c-Myb as the major transcription factors of *Sphk1* gene and that Sphk1 at least partially plays a role in modulating differentiation sensitivity byHMBA.

Materials and Methods

Cell lines: Mouse Friend erythroleukemia cell line (original Friend cells) was reported previously (5), and its HMBA-resistant subline (Friend R) was established by continuous treatment with HMBA.

Erythroid differentiation: Chemical induction was performed with 5mM Hexamethylene-bisacetamide (HMBA). Hemoglobin-positive cells were detected by liquid benzidine staining.

Sphk enzyme activity was measured as described previously (6).

Real time RT-PCR was previously described previously (7).

Western Blotting: Anti-SPHK2, anti-FLI-1, anti-PU.1, anti-c-MYB, anti-GATA-1, and anti-GATA-2 antibody were purchased from Santa Cruz Biotechnology. Anti-β-actin antibody was purchased from BioVision. Anti-mouse SPHK1 antibody was described before (8).

Sphk1 promoter analysis: To determine the transcription initiation point of *Sphk1* in Friend cells, RNA ligase-mediated rapid amplification of 5'-cDNA ends (5-RACE) was performed. Based on these data, the 1.7-kb 5'-promoter region of mouse SPHK1 gene was obtained by PCR methods and inserted into pGL3 basic vector. Eight deletion mutants and 4 mutation-inserted vectors were prepared.

Electrophoresis mobility shift assay (EMSA): Nuclear extract was prepared from original Friend cells or Friend R cells with or without HMBA treatment for 48 h. EMSA was performed according to the method previously described previously (9).

Chromatin immunoprecipitation (ChIP) assay was carried out as described previously (10).

Transient transfection of siRNA: Friend cells were transfected with siRNA against c-Myb, nonspecific siRNA or c-Myb expression vector by the lipofection method.

Results

SPHK1 and SPHK2 expression of various mouse cell lines

Sphk1 mRNA of Friend cells was much higher than other mouse cell lines analyzed, whereas Sphk2 mRNA did not. This tendency was also demonstrated in Western blotting.

Effects of SPHK1 and SPHK2 overexpression

To examine the role of Sphks in Friend cell survival, proliferation and differentiation, we established several subclones of Friend cells. SPHK1-wild-type (SPHK1-WT) demonstrated higher proliferation and resistance against serum depletion-induced cell death. Furthermore, erythroid differentiation was delayed as compared with original Friend cells. On the contrary, SPHK1-dominant-negative (SPHK1-DN) showed lower proliferation in culture with FCS and higher apoptosis in serum-depleted culture. We also established WT- and DN-SPHK2 transfectants. Cell proliferation was delayed in SPHK2-WT and apoptosis induced with serum depletion was reduced in SPHK2-DN cells.

HMBA-induced erythroid differentiation of Friend cells and its resistant clone, Friend R

We examined HMBA-induced differentiation of original Friend cell and the resistant clone, R cells. After 4 days incubation with 5mM HMBA, Friend cells demonstrated almost 100 % hemoglobin positive, whereas Friend R did not show any hemoglobin positivity. Friend cells gradually decreased cell proliferation during HMBA treatment, whereas R cells continued to proliferate even in HMBA (+) medium. R cells showed higher Sphk1 mRNA and delayed and much milder decrease of Sphk1 enzyme activity by HMBA compared with

original cells. To prove the positive effects on *Sphk1* expression by proto-oncogenes, we examined FlI-1 and Pu.1 proteins. c-MYB expression was also examined because it has been reported that differentiation-resistant Friend cell lines can not completely down-regulate c-MYB expression with DMSO. Interestingly, c-MYB protein stayed high in HMBA-treated R cells, whereas FLI-1 and PU.1 decreased in HMBA-treated Friend R cells, suggesting the positive relationship between HMBA resistance and *Sphk1* overexpression stimulated by c-Myb transcription factor.

5' promoter analysis

Promoter analysis using various lengths of reporter vector revealed that the region between – 53 and -4 bp from the first exon is sufficient for the promoter activity of Friend cells. We further analyzed this region by inserting several mutations to the putative transcription factor binding sites. Results revealed that the proximal Myb-binding site was the most important within this area, through other Myb- and Ets-binding site also demonstrates some promoter activity.

EMSA

The promoter region containing three Myb-binding sites and one Ets-binding site was used as the biotin-labeled probe for EMSA. Nuclear extracts of Friend cells produced 3 bands. Bands 2 and 3 were competed with the same non-labeled probe, suggesting the specificity of these band formation. Anti-c-Myb antibody decreased band 3, although not completely. We produced c-Myb protein from GST-c-MYB fusion protein. It clearly shows that band 3 contained c-Myb protein. Intriguingly, HMBA treated Friend cells but not HMBA-treated Friend R cells demonstrated the reduction of band 3. Furthermore, Band 1 increased its intensity in both HMBA-treated Friend cells and Friend R cells, and increased band 2 appeared only in HMBA-treated Friend R cells, suggesting the complex occupation of these binding sites with multiple transcription factors.

ChIP assay and siRNA for c-MYB or c-MYB expression vector transfection

We performed the ChIP assay covering this region. In vivo binding of c-MYB was clearly shown. Inhibition and overexpression of c-MYB using siRNA for c-MYB and c-MYB expression vector,. Thus, we proved that c-MYB level could affect SPHK1 expression significantly.

Discussion

In the present study, we analyzed the sequential change and the pathophysiological roles of SPHK family proteins during HMBA-induced differentiation of Friend cells. Our analyses confirmed the previous paper by le Scolan et al. (4) reporting high *Sphk1* expression of Friend cells. Moreover, in our current study, *Sphk1* rapidly decreased during HMBA-induced differentiation of original Friend cells, whereas its HMBA-resistant variant, R cells, did not, suggesting the important role of *Sphk1* in leukemic proliferation of Friend cells and the sensitivity to chemical inducers. By using stable transformants of wild type and dominant negative SPHK1 and SPHK2, we also provided the evidence that *Sphk1* and *Sphk2* play different roles in Friend cells and the validity of proposed sphingolipid rheostat model.

Our present results including the comparison of cellular proteins of HMBA-treated original Friend cells and R cells, the promoter analysis of *Sphk1*, EMSA, and ChIP assay revealed that *Sphk1* expression was mostly regulated by c-Myb and Myb-binding sites of the 5'-*Sphk1* promoter. Moreover, our EMSA exhibiting the binding of Myb protein binding in vivo and the decrease of Myb binding in HMBA-treated original Friend cells but not in HMBA-treated R cells strongly suggest that Myb/SPHK1 signaling modulates the differentiation induction sensitivity of Friend cells.

Conclusions

In Friend cells, c-Myb plays a major role in *Sphk1* transcription and that Sphk1 level can modulates HMBA-induced commitment to terminal cell differentiation.

References

[1]Fahy E, Subramaniam S, Glass CK, Merrill AH, Jr., Murphy RC*, et al.* A comprehensive classification system for lipids. *J Lipid Res* 2005; **46**(5):839-861.

[2]Hannun YA, Obeid LM. Principles of bioactive lipid signalling: lessons from sphingolipids. *Nat Rev Mol Cell Biol* 2008;**9**(2):139-150.

[3]Moreau-Gachelin F. Multi-stage Friend murine erythroleukemia: molecular insights into oncogenic cooperation. *Retrovirology* 2008;**5**:99.

[4]Le Scolan E, Pchejetski D, Banno Y, Denis N, Vainchenker W*, et al.* Overexpression of sphingosine kinase 1 is an oncogenic event in erythroleukemic progression. *Blood* 2005;106(5):1808-1816.

[5]Murate T, Kaneda T, Rifkind RA, Marks PA. Inducer-mediated commitment of murine erythroleukemia cells to terminal cell division: the expression of commitment. *Proc Natl Acad Sci USA* 1984;**81**(11):3394-3398.

[6]Nakade Y, Banno Y, K TK, Hagiwara K, Sobue S, Koda M*, et al.* Regulation of sphingosine kinase 1 gene expression by protein kinase C in a human leukemia cell line, MEG-O1. *Biochim Biophys Acta* 2003;**1635**(2-3):104-116.

[7]Sobue S, Iwasaki T, Sugisaki C, Nagata K, Kikuchi R, Murakami M*, et al.* Quantitative RT-PCR analysis of sphingolipid metabolic enzymes in acute leukemia and myelodysplastic syndromes. *Leukemia* 2006;**20**(11):2042-2046.

[8]Murate T, Banno Y, K TK, Watanabe K, Mori N,Wada A*, et al.* Cell type-specific localization of sphingosine kinase 1a in human tissues. *J Histochem Cytochem* 2001;**49**(7):845-855.

[9]Sobue S, Murakami M, Banno Y, Ito H, Kimura A, Gao S*, et al.* v-Src oncogene product increases sphingosine kinase 1 expression through mRNA stabilization: alteration of AU-rich element-binding proteins. *Oncogene* 2008;**27**(46):6023-6033.

[10]Ito H, Murakami M, Hagiwara K, Kobayashi M*, et al.* Heterogeneous sphingosine-1-phosphate lyase gene expression and its regulatory mechanism in human lung cancer cell lines. *Biochim Biophys Acta* Mar;**1811**(3):119-128.

Author address

E-Mail: kobayashi.misa@a.mbox.nagoya-u.ac.jp

A SIGNAL PEPTIDE MUTATION OF ENDOGLIN ASSOCIATED WITH HHT

Atsuo Suzuki[1, 6)], Yuhri Miyawaki[1)], Junko Fujita[1)], Asuka Maki[1)], Eriko Okuyama[1)], Moe Murata[1)], Akira Takagi[1, 2)], Takashi Murate[1, 2)],Masaaki Teranishi[3)], Tadashi Matsushita[4)], Hidehiko Saito[5)] and Tetsuhito Kojima[1, 2)]

1) Department of Pathophysiological Laboratory Sciences, Nagoya University Graduate School of Medicine
2) Department of Medical Technology, Nagoya University School of Health Sciences
3) Department of Otorhinolaryngology, Nagoya University Graduate School of Medicine
4) Division of Transfusion Medicine, Nagoya University Hospital
5) National Hospital Organization Nagoya Medical Center
6) Japan Society for the Promotion of Science Research Fellow

Introduction

Hereditary hemorrhagic telangiectasia (HHT), also known as Osler-Rendu-Weber syndrome, is an inherited autosomal dominant vascular dysplasia with a frequency of 1 in 10,000 and exhibits age-related penetrance with variable expressivity [1-3]. The most common clinical manifestations involve the development of vascular abnormalities seen as telangiectases on skin and lesions in nasal mucosa that readily bleed. Further clinical manifestations are pulmonary, cerebral, hepatic and, in rare cases, spinal cord arteriovenous malformations. These may cause serious complications such as stroke, brain abscess, hemorrhage, or venous thromboembolism [4-6].

HHT type 1 (HHT1) is caused by a mutation in the gene encoding endoglin (*ENG*) located on the long arm of chromosome 9 (9q34) [7-9]. HHT type 2 (HHT2) is caused by a mutation in the activin-like kinase receptor 1 (ALK1) gene (*ACVRL1*) located on the long arm of chromosome 12 (12q13) [10-12]. Endoglin is a homodimeric integral membrane glycoprotein that interacts with signaling receptor complexes for several members of the transforming growth factor-β (TGF-β) superfamily, and composed of disulfide-linked 90-kDa subunits [13-15]. It is expressed primarily in the vascular endothelial cells of capillaries, arterioles, and venules, as well as in activated monocytes, syncytiotrophoblasts, and some leukemic cells. ALK1 is also expressed on endothelial cells, and is a type I receptor of the TGF-β superfamily [16]. TGF-β family cytokines are multifunctional proteins that regulate proliferation, differentiation, migration, adhesion and apoptosis of various cell types [5].

To date, 282 different mutations have been reported in the *ENG* gene and 246 distinct mutations in the *ACVRL1* gene (human gene mutation database: HGMD [17]). Some missense mutations in the signal peptide region of endoglin have been reported, but their molecular basis has yet to be investigated in detail. In this study, we analyzed the *ENG* gene in a Japanese patient with HHT, and found a novel missense mutation in the signal peptide region of endoglin. We further investigated the molecular basis of HHT in the patient through expression analyses of the mutant endoglin in COS-1 cells.

Materials and Methods

Sample preparation

Ethical approval for this study was obtained from the Ethics Committee of the Nagoya University School of Medicine. Citrated blood samples were obtained from the patient and his sister with informed consent. Genomic DNA was isolated from the peripheral leukocytes by phenol extraction.

Polymerase Chain Reaction (PCR) and DNA sequencing

The protein-coding exons and exon-intron boundaries of *ENG* and *ACVRL1* were amplified by the polymerase chain reaction (PCR) using gene-specific primers.

Cell culture

African green monkey kidney COS-1 cells were purchased from the American Type Culture Collection. Human endothelium-like EAhy926 cells were generously donated by Dr. Cora-Jean S. Edgell (University of North Carolina). The cells were cultured in Dulbecco's Modified Eagle's Medium (DMEM) supplemented with 10% fetal bovine serum (FBS).

Transient transfection

COS-1 cells were seeded, and the respective vector was transfected using Lipofectoamine2000 reagent according to the manufacturer's directions. Following experiments were performed at 48 h after transfection.

Western Blot analysis

The transfected cells were lysed with or without β-mercaptoethanol (β-ME), boiled, and subjected to 10% SDS-PAGE followed by Western blotting.

Flow cytometry analysis

COS-1 cells were transiently transfected with 1μg of pL-ENG^{WT} or pL-ENG^{L13Q}, and harvested using 1mM EDTA in PBS after 48hr. The cells were washed, and incubated with anti-endoglin antibody or isotype-matched rabbit IgG (10μg/mL). Anti-rabbit IgG-Alexa488 antibody was incubated and the cells were analyzed by flow cytometer.

Immunofluorescence microscopy

The trasnfected COS-1 cells were replated and grown on 18x18mm cover glasses that were coated with collagen I. Forty-eight hours after transfection, the cells were fixed in cold methanol, and permeabilized with cold acetone. Antibodies used in immunofluorescence were as follows; rabbit anti-endoglin antibody, mouse anti-alpha 1 sodium potassium ATPase antibody, anti-protein disulfide isomerase (PDI) antibody, anti-rabbit IgG-Alexa488 antibody, anti-mouse IgG-Alexa555 antibody.

Results

Case report

The patient was a 61-year-old Japanese man, and showed epistaxis, telangiectases, lung arteriovenous malformations and familiar bleeding history, he was diagnosed with HHT according to Curaçao criteria [5] .

Sequencing of ENG and ACVRL1

Direct sequencing of the proband's *ENG* and *ACVRL1* genes revealed a novel missense mutation in exon 1 of *ENG* as a heterozygous form, but no mutation in *ACVRL1*. The mutation was a T-to-A transversion at nucleotide 38 in the coding sequence of *ENG* (c.38T>A), replacing leucine 13 (CTG) with a glutamine (CAG) (p.Leu13Gln) in the hydrophobic core region of the endoglin signal peptide.

Western blot analysis of recombinant endoglins expressed in COS-1 cells

To examine the effects of the L13Q missense mutation on the structure and function of endoglins, we expressed the mutant and wild-type endoglins (long-form; L-ENG, short-form; S-ENG) in COS-1 cells, and compared them by Western blotting. Under reducing conditions, the recombinant wild-type L- and S-ENG showed 3 bands, whereas the L13Q mutant showed only a smaller band. The endogenous endoglin from EAhy926 cells possessed a single band equal in size to a larger band of recombinant L-ENG. Under non-reducing conditions, Western blotting revealed that the wild-type L-ENG showed two bands representing a protein dimer, which were similar in size to the endogenous endoglin from EAhy926 cells. However, the L13Q mutant mostly retained a smaller 60kDa band at 72hr after transfection, indicating that the L13Q mutation impaired the dimerization of recombinant endoglin.

Impaired cell surface expression of the L13Q mutant

To analyze whether recombinant endoglins express on the cell surface, we performed flow cytometry using anti-endoglin antibody. The results showed that over 25% of the cells transfected with wild-type endoglin-expression vector were positive for endoglin expression on the cell surface, whereas less than 3% of the cells transfected with L13Q mutant endoglin-expression vector were positive.

We tested the cell-surface expression of recombinant endoglins by immunofluorescence analysis for Na-K-ATPase using as a trasnmembrane marker. As a result, wild-type endoglin was detected all over the cell bodies and co-localized with Na-K-ATPase on a part of the cell surface, but we could detect no positive endoglin signal of L13Q mutant.

Distribution of recombinant endoglins

To investigate the intracellular distribution of the recombinant endoglins, we performed immunofluorescence microscopy for endoglin, together with that for endoplasmic reticulum (ER) by using an antibody against protein disulfide isomerase (PDI). In the COS-1 cells, wild-type endoglin signals were detected in the entire area of the cell and co-localized with ER marker PDI in the peri-nuclear region. Meanwhile, the L13Q mutant endoglin was stained in a scattered pattern and almost never co-localize with PDI.

Discussion

In this study, we investigated the molecular basis of HHT in a Japanese patient, and identified a novel missense mutation in the *ENG* gene (c.38T>A, p.Leu13Gln), located in the hydrophobic core of the endoglin signal peptide. There are some reports of missense mutations in the endoglin signal peptide [3, 18-22], but their molecular basis has yet to be investigated in detail.

To examine effects of the L13Q mutation on the structure and function of endoglin, we performed transient expression experiments for the recombinant endoglins in COS-1 cells. In Western blotting under non-reducing conditions, the wild-type recombinant endoglins appeared to be expressed as a protein dimer, whereas the L13Q mutant remained as a non-glycosylated precursor. It was speculated that the L13Q mutation might impair post-translational processing of endoglin such as glycosylation and dimerization, probably due to a destroyed function of the signal peptide. Flow cytometry and immunofluorescent microscopy analyses of the recombinant endoglins also demonstrated that the wild-type endoglins were expressed on the cell surface and co-localized with the ER, but the L13Q mutant did not. These results suggested that the L13Q mutation might severely impair endoglin expression on the cell surface..

Conclusions

We identified a novel missense mutation in the hydrophobic core of the endoglin signal peptide (p.Leu13Gln), which is suggested to be responsible for HHT in the patient.

References

[1] Guttmacher AE et al. N Engl J Med, 1995, 333(14): 918-24
[2] Plauchu H et al. Am J Med Genet, 1989, 32(3): 291-7
[3] Berg J et al. J Med Genet, 2003, 40(8): 585-90
[4] Shovlin CL et al. Thromb Haemost, 1997, 78(1): 145-50
[5] Fernandez-L A et al. Clin Med Res, 2006, 4(1): 66-78
[6] Shovlin CL et al. Thromb Haemost, 2007, 98(5): 1031-9
[7] McDonald MT at al. Nat Genet, 1994, 6(2): 197-204
[8] Shovlin CL et al. Nat Genet, 1994, 6(2): 205-9
[9] McAllister KA et al. Nat Genet, 1994, 8(4): 345-51
[10] Vincent P et al. Hum Mol Genet, 1995, 4(5): 945-9
[11] Johnson DW et al. Genome Res, 1995, 5(1): 21-8
[12] Johnson DW et al. Nat Genet, 1996, 13(2): 189-95
[13] Shovlin CL et al. Am J Hum Genet, 1997, 61(1): 68-79
[14] Lux A et al. J Biol Chem, 1999, 274(15): 9984-92
[15] Gougos A et al. J Immunol, 1988, 141(6): 1925-33
[16] Attisano L et al. Cell, 1993, 75(4): 1925-33
[17] http://www.hgmd.cf.ac.uk/ac/all.php
[18] Galloine CJ et al. Hum Mutat, 1998, 11(4): 286-94
[19] Letteboer TG et al. Hum Genet, 2005, 116(1-2): 8-16
[20] Bourdeau A et al. Trends Cardiovasc Med, 2000, 10(7): 279-85
[21] Lesca G et al. Hum Mutat, 2004, 23(4): 288-99
[22] Bossler AD et al. Hum Mutat, 2006, 27(7): 667-75

Author address

E-mail: suzuki.atsuo@d.mbox.nagoya-u.ac.jp

Anthocyanin inhibits CagA and VacA toxins via SecA suppression in *Helicobacter pylori*

Sa-Hyun Kim[1], Min Park[1], Gyusang Lee[1], Woo-Duck Seo[2], Sang-Ick Han[2], and Jong-Bae Kim[1]
[1]Department of Biomedical Laboratory Science, College of Health Science, Yonsei University, Wonju, Korea
[2]Department of Functional Crop, NICS, Miryang, Korea

INTRODUCTION: Anthocyanin from various crops and fruits are known as an antioxidant, antibacterial and antiviral agent. It was reported as a potential anti-microbial agent in *Helicobacter pylori*. However it has never known that anthocyanin is a toxin inhibitor for *H. pylori*. We examined that the biosynthesis of cytotoxin associated protein A (CagA) and vacuolating toxin A (VacA) can be suppressed by anthocyanin in vitro.

METHODS: *H. pylori* reference strain (ATCC 49503, CagA+/VacA+) was used in this examination. Bacteria were subcultured in the Brucella agar medium with 10% fetal bovine serum at 37℃/ 10% CO_2 incubator. And cultured *H. pylori* cells were incubated in the Mueller-Hinton broth with or without anthocyanin 3.4 days. Anthocyanin was administrated to the culture broth as the concentration of 100 micromoles. Next, the two dimensional electrophoresis (2DE) was performed to compare the changed protein profiles of *H. pylori* without and with anthocyanin. This 2DE data were confirmed by western blotting, and the anti-CagA mouse monoclonal antibody, the anti-VacA rabbit polyclonal antibody, and anti-*H. pylori* polyclonal rabbit antibody which we produced were used in immunoblottings. To examine the start points of the inhibition for CagA and VacA toxins, the RT-PCR and PCR were performed, these data were compared with the data of western blotting.

RESULTS: Two dimensional electrophoresis (2DE) profiles of *H. pylori* reference strain (ATCC 49503, CagA+/VacA+) demonstrated that anthocyanin can inhibit the expression of SecA which regulates type Ⅳ, and Ⅴ secretion systems of *H. pylori*. The biosynthesis of CagA and VacA can be suppressed via SecA inhibition because CagA and VacA is regulated by type Ⅳ, and Ⅴ secretion system, respectively. Immunoblotting was performed and confirmed the biosynthesis of CagA and VacA were suppressed in *H. pylori* with the treatment of anthocyanin, also.

CONCLUSION: For the first time, our data demonstrate that anthocyanin can be an inhibitor for *H. pylori* toxons, CagA and VacA via SecA suppression. Further study should be needed whether anthocyanin might be effective in the suppression of the biosynthesis of CagA and VacA toxin of *H. pylori* in vivo. If so, anthocyanin could be used to reduce the gastric inflammation or stomach cancer due to *H. pylori* infection.

Molecular Diagnostic Approach for Screening Latent Tuberculosis Infection (LTBI)

Sunghyun Kim[1+], Young Keun Kim[2+], Hyejon Lee[3], Jang Eun Cho[4], Young Mi Kim[3], Hyunjung Kim[3], Sang-Nae Cho[3], and Hyeyoung Lee[1*]

[1] Department of Biomedical Laboratory Science, College of Health Sciences, Yonsei University,

[2] Department of Internal Medicine, Yonsei University Wonju College of Medicine, Wonju, Gangwon,

[3] Department of Microbiology, College of Medicine, Yonsei University, Seoul,

[4]Department of Biomedical Laboratory Science, Daegu Health College, Daegu, Republic of Korea

INTRODUCTION: Tuberculosis (TB) continues to be one of the most critical infectious disease and causes three million deaths annually. About one-third of world population is latently infected with *Mycobacterium tuberculosis* (MTB). Recently, new immunodiagnostic tests for detection of latent TB infection (LTBI) called interferon gamma release assay (IGRA) have been developed. Commercially available IGRA tests have showed higher specificity and sensitivity than conventional tuberculin skin test (TST). However, IGRA tests have some limitations. In order to overcome these limitations, we developed alternative IGRA using reverse transcriptase (RT)-PCR.

METHODS: Total of 101 TB suspects were enrolled for this study. All suspects were diagnosed by various clinical laboratory tests (AFB sputum smear, mycobacterial culture, chest radiographs, histopathologic technique, TB/NTM real-time PCR). Whole bloods of all suspects were collected for performing IGRA using QuantiFERON®-TB Gold In-Tube ELISA kit (Cellestis, Victoria, Australia) and *IFN-γ mRNA RT-PCR.*

RESULTS: In active pulmonary or extrapulmonary TB patients, IGRA (90%, 100%) showed higher positivity than IFN-γ mRNA RT-PCR (both 80%). However, in previous TB patients, IFN-γ mRNA RT-PCR (83.3%) showed higher positivity than IGRA (50%). In latent TB or non-TB suspects, IFN-γ mRNA RT-PCR (46.6%) also showed higher positivity than IGRA (30.1%). In patients who have infected with nontuberculous mycobacteria (NTM), both IFN-γ mRNA RT-PCR and IGRA have shown 100% negativity. Furthermore, IFN-γ mRNA RT-PCR was also able to distinguish between MTB infection and NTM infection. In 6 previous TB patients, IGRA showed 1 (16.7%) indeterminate result, however, it was positive when performed with IFN-γ mRNA RT-PCR. And also among 73 latent TB or non-TB subjects, IGRA showed 7 (9.6%) indeterminate results, among them 3 (42.9%) were positive and 4 (57.1%) were negative when performed with IFN-γ mRNA RT-PCR.

CONCLUSION: Although IFN-γ mRNA RT-PCR has shown lower sensitivity in detection of active TB cases, it showed higher sensitivity in detecting latent TB suspects than IGRA. The assay developed in this study reduces turn-around time, cost for test, volume of blood and is not affected by the number of samples.

Target–specific gene delivery by anti-EGFR immunonanoparticles to tumor cells

Jung Seok Kim, Yeon Kyung Lee, Hwa Yeon Jung, Young Eun Shin and Young Serk Park.
Department of Biomedical Laboratory Science, College of Health Sciences,
Yonsei University, Wonju, Republic of Korea

INTRODUCTION: Gene therapy has been considered as a promising approach in the treatment of varied disease as the understaing of genetic basis of diseases is expanded. The epidermal growth factor receptor (EGFR) has been recognized as a therapeutic target molecule for cancer treatment. Elevated levels of EGFR are found on varied types of tumors and have been proposed as a prognostic marker for cancer progression and survival. Therefore, antibodies recognizing EGFR such as Cetuximab and Panitumumab have been widely applied for targeting of vehicles carrying therapeutic genes (pDNA or siRNA) to EGFR-expressing cancer cells. In this study, we have developed EGFR-targeted gene delivery systems (immunolipoplexes and immunoviroplexes) by conjugating anti-EGFR antibodies (Cetuximab) to liposomal surface. The plasmid DNA was effectively complexed with those nanoparticles and then efficiently transferred to varied EGFR-positive cancer cells (A549 and SK-OV-3). In this report, we would like to introduce preparation of anti-EGFR immunonanopaticles containing pDNA and their effectiveness in pDNA transfection to EGFR-positive cells *in vitro* and *in vivo.*

METHODS: Immunolipoplexes and immuniviroplexes were prepared by conjugation of Cetuximab molecules to cationic lipoplexes and cationic Sendai F/HN viroplexes, respectively. Their EGFR-mediated cell bindings and gene transfection were tested in EGFR-positive A549 human lung cancer cells and SK-OV-3 human ovarian cancer, using flow cytometry, fluorescence microscopic analysis, and assay of transgene (luciferase) expression. The anti-EGFR immunoliplexes and immunoviroplexes were intravenously administered to SK-OV-3-xenografted nude mice. Their cellular uptake and *in vivo* gene transfection were assessed by assay of transgene expression and fluorescence microscopic examination.

RESULTS: Anti-EGFR immunonanoparticles showed selective binding to EGFR-positive cells (A549 and SK-OV-3) and also exhibited higher gene expression in EGFR-positive cells than in EGFR-negative cells. Especially, the anti-EGFR immunoviroplexes exhibited more efficient pDNA transfection than the anti-EGFR immunolipoplexes. The anti-EGFR immunonanoparticles were able to enhance transfection to EGFR-positive SK-OV-3 tumor cells xenografted in nude mice, compared with the bare lipoplexes. Under the same transfection conditions, the anti-EGFR immunonaoplexes and immunoviroplexes induced 100-fold and 400-fold higher gene expression in the tumor than the bare cationic lipoplexes, respectively. At the same time, the anti-EGFR immunonanoplexes showed higher accumulation in the tumor tissues. Among the two systems, the anti-EGFR immune-viroplexes appeared to be more effective in EGFR-mediated *in vivo* pDNA transfection than the anti-EGFR immunolipoplexes.

CONCLUSION: Anti-EGFR immunonanoparticles were able to transfer pDNA more efficiently and selectively to EGFR-expressing tumor cells. Especially, the anti-EGFR immunoviroplexes exhibited higher *in vitro* and *in vivo* pDNA transfection than the anti-EGFR immunolipoplexes. This study suggests that anti-EGFR immunonanoparticles can be a useful system for therapeutic gene delivery to EGFR-overexpressing cancer cells.

Molecular Detection of Circulating Tumor Cells in Peripheral Blood of Breast Cancer Patients

[1]Park Sangjung, [2]Han Hyunju, [2]Kim Seung Il and [1]Lee Hyeyoung.

[1]Department of Biomedical Laboratory Science, College of Health Sciences, Yonsei University, Gangwon
[2]Yonsei Cancer Center, College of Medicine, Yonsei University, Seoul, Republic of Korea

INTRODUCTION: Breast cancer is considered as a systemic disease because it has higher metastatic property than other types of cancer. Metastasis of cancer is the leading cause of cancer-related deaths. In metastatic stage of cancer, cancer cell departs from primary tumor site and moves to other organs through the blood stream. Thus, detection of circulating tumor cells (CTC) in peripheral blood of cancer patients is very important for prognostic and predictive significance. The presence of CTCs in the blood of a cancer patient is associated with a worse prognosis. Therefore, diagnosis of CTC in early stage of breast cancer patients is important to predict prognosis of patients. In this study, we identified specific genetic markers useful for CTC detection in peripheral blood of early breast cancer patients using Real-time RT-PCR, which will be valuable for monitoring the metastatic stage and to predict prognosis of patients.

METHODS: A total of 20 female patients with metastatic breast cancer being treated at the Yonsei Severance Hospital between 2010 and 2011 were enrolled in this study. Peripheral blood was collected from the patients during surgical therapy. Peripheral blood (10ml in EDTA) was obtained from breast cancer patients and healthy donor. Blood cell lysis reagent removed RBC in blood. Total RNA was extracted from blood samples and cell lines using Trizol according to the manufacturer's protocol. Real-time RT-PCR targeting cytokeratin (CK19), Ki67 and Human Epithelial Growth Factor Receptor (HER-2) were performed in final volume of 20 ul. Each gene expression normalized using TBP gene. The cut-off value of each assay was determined based on the results of healthy donors.

RESULTS: The sensitivities of real-time RT-PCR for detection of each marker were performed. Sensitivity of real-time RT-PCR for targeting CK19 was 100 cells, while those of HER-2 and Ki67 were 10 cells. The cut-off values for each assay were decided based on the expression levels of normal controls. Subsequently, the real-time RT-PCRs targeting CK19, HER-2, and Ki67 were performed using blood samples derived from 20 female patients with metastatic breast cancer. The results showed that among 20 patients, 20 percents (4/20) had CK19 positive rates and another 20 percents (4/20) had HER-2 positive rate. On the other hand, 70 percents (14/20) had Ki67 positive rate. Patients who were only single marker expression were 10: 8 patients expressed only Ki67 and 2 patients expressed only HER2. Six patients expressed two markers together, and 4 patients expressed CK19 and Ki67. Two patients were HER2 and Ki67 co-expression. Lastly, 4 patients did not express any markers.

CONCLUSION: Among 20 patients, 16 patients (80 %) were detected to contain multiple markers by using real-time RT-PCR. Therefore, real-time RT-PCR employing multiple CTC markers seems to be more effective than single marker for diagnosis of CTC.

Real-time nucleic acid sequence based amplification (NASBA) for detection of influenza A virus subtypes

Jaewon Lim[1], Yoonjung Cho[1], In Soo Lee[2], Hyeeun Bang[1], Hyeyoung Lee[1] and Tae Ue Kim[1]
[1]Department of Biomedical Laboratory Science, College of Health Science,
Yonsei University, Wonju, 220-710
[2]Department of Clinical Laboratory Science, Hyejeon College, Hongseong, 350-702

INTRODUCTION: Influenza A virus of the *Orthomyxoviridae* family is a contagious respiratory pathogen that continues to evolve and burden in the human public health. It is able to spread efficiently from human to human have the potential to cause pandemics with significant morbidity and mortality. It has been estimated that every year about 500 million people are infected with this virus, causing about approximately 0.5 million people deaths worldwide. Influenza A viruses are classified into different subtypes by Antigenicity base on their hemagglutinin (HA) and neuraminidase (NA) proteins. The sudden emergence of influenza A virus subtypes and access for epidemiological analysis of this subtypes demanded a rapid development of specific diagnostic tools. Also, rapid identification of the subtypes can help to determine the antiviral treatment, because the different subtypes have a different antiviral drug resistance patterns.

METHOD: In this study, our aim is to detection of influenza A virus subtypes by using real-time NASBA which has high sensitivity and specificity through molecular beacon. Real-time NASBA is the method that able to shorten the time compare to other molecular diagnostic tools and is performed by isothermal condition. We selected major pandemic influenza A virus subtypes H3N2 and H5N1. Then, three influenza A virus gene fragments were targeted, heamgglutinin (HA) gene, neuraminidase (NA) gene and Matrix protein (M) gene, respectively. M gene is distinguished influenza A virus from other influenza virus. We designed specific primers and molecular beacons for each targeted RNA segments.

RESULT: We performed RT-PCR with each of subtype reference genes specific primer to confirm specificity and quantify the amplicons. M gene, H3N2 and H5N1 genes primer have good specificity; however H3N2 NA2 gene primer has shown lower specificity. PCR product which has amplified by H5N1 gene primer has shown lower relatively sensitivity then others. To confirm the optimal condition of real-time NASBA, we tested with positive control and negative control. It was confirmed that optimal cut-off signal value was 2, and then the amplification signals of each gene have rise up since 21 to 41 minutes. We performed each of subtype HA/NA gene specific molecular beacon to confirm the specificity. As a result, molecular beacon detecting all subtypes of HA/NA genes have higher specificity.

CONCLUSION: the real-time NASBA was able to detect and distinguish H3N2/H5N1 subtypes from other subtypes of influenza A virus. Also, the specificity and the sensitivity of the method using real-time NASBA were higher then that of RT-PCR. This study suggests that rapid detection of neo-appearance pandemic influenza A virus using real-time NASBA has the potential to determine the subtypes of respiratory pathogen.